Analysis of synapse-level neuronal morphology in human post-mortem brain tissue

Running Title: Neuron morphology in human brain

Sujan C. Das[1], Danli Chen[1], W. Brandon Callor[3], Eric Christensen[3], Hilary Coon[1, *], Megan E. Williams[2, *]

[1]Department of Psychiatry, University of Utah School of Medicine, Salt Lake City, UT84112, USA

[2]Department of Neurobiology and Anatomy, University of Utah School of Medicine, UT84112, USA

[3]Utah State Office of Medical Examiner, Utah Department of Health, Salt Lake City, UT, USA

[*]**Correspondence**

megan.williams@neuro.utah.edu

hilary.coon@hsc.utah.edu

Acknowledgments and Funding:

This work was supported by grants from the National Institute of Mental Health R01MH099134 (HC) and R01MH105426 (MEW) and the University of Utah Medical School Psychiatry Department Research Fund (SD). We especially thank the Utah State Office of the Medical Examiner staff who made this study possible.

ABSTRACT

Many cognitive and psychiatric disorders are thought to be disorders of the synapse, yet the precise synapse defects underlying these disorders remain unknown. Because synapses are highly specialized anatomical structures, defects in synapse formation and function can often be observed as changes in micro-scale neuroanatomy. Unfortunately, few methods are available for accurate analysis of synapses in human post-mortem tissues. Here, we present a new methodological pipeline for assessing synapse-level neuron morphology in human post-mortem tissue that is accurate, rapid, and relatively inexpensive. Our method uses small tissue blocks from postmortem human brains, immersion fixation, single cell resolution by dye labeling, and confocal microscopy. As proof of principle, we analyzed pre- and postsynaptic structures from hippocampi of 13 individuals aged 4 months to 71 years. Our results suggest that postsynaptic CA1 dendritic spine shape and density are stable across ages, while presynaptic DG mossy fiber boutons undergo significant structural rearrangements with normal aging. This suggests that mossy fiber synapses, which play a major role in learning and memory, remain dynamic throughout life. Importantly, we find no effect of postmortem intervals up to 28 hours on neuron morphology. Thus, the ease of our new protocol should facilitate higher powered studies of human synapse structure in healthy and diseased states.

Keywords: Hippocampus, Dendritic Spine, Mossy Fiber Bouton, Post-mortem, Synapse

1 | INTRODUCTION

Neuropsychiatric disorders constitute a major health burden globally. Although the exact molecular mechanisms are unknown, altered neuronal connectivity is widely thought to underlie the neuropathology of most psychiatric disorders (Penzes, Cahill, Jones, VanLeeuwen, & Woolfrey, 2011; Radley et al., 2008). Studies using advanced genetic methods including genome-wide association studies, whole genome sequencing, exome sequencing, and enrichment analysis indicate that genes altered in neuropsychiatric disorders frequently encode molecules that mediate synapse formation and function (Forrest, Parnell, & Penzes, 2018). Because synapse structure and function are tightly linked, alterations in synaptic function often results in structural changes that can be observed using light microscopy. Some of the synaptic structures that can be affected include axonal and dendritic arborizations, pre-synaptic boutons, and post-synaptic dendritic spines. In particular, dendritic spines are finger-like projections protruding from the dendritic shaft that house critical post-synaptic elements of glutamatergic synapses. Electron microscopy indicates that the vast majority (>95%) of dendritic spines contain an asymmetric synapse (Arellano, Espinosa, Fairen, Yuste, & DeFelipe, 2007; Harris, Jensen, & Tsao, 1992). Moreover, spine size positively correlates with synapse size and synaptic strength (Berry & Nedivi, 2017; Harris, Fiala, & Ostroff, 2003). Because spines are large enough to be resolved by light microscopy, analysis of spine density and shape is a commonly used and reliable proxy for excitatory synapse density and function.

Although animal models are useful for studying psychiatric disorders, they cannot mimic human neuropathology to the full extent. Thus, human post-mortem tissues provide an opportunity to study synapse-level connectivity patterns in psychiatric disorders. However, cellular and subcellular imaging in human post-mortem tissues is hindered by the inability to rapidly fix human

tissue by aldehyde perfusion. The most widely used method for analyzing synapse morphology in the postmortem human brain tissue is dendritic spine analysis after Golgi staining. However, Golgi staining can underestimate spine density by as much as three-fold because it uses two-dimensional imaging (Shen, Sesack, Toda, & Kalivas, 2008). Electron microscopy is the gold standard for synapse imaging but it is expensive, time-consuming, and requires specialized technical skills. Single cell microinjection of fluorescent dyes followed by confocal microscopy generates spectacular synapse-resolution, three-dimensional images of single neurons (Benavides-Piccione, Fernaud-Espinosa, Robles, Yuste, & DeFelipe, 2013; Merino-Serrais et al., 2013). However, even in mice, microinjection can be a fickle method that requires a precise level of fixation, does not label axons well, and works best in human tissues with very short post-mortem intervals. Taken together, all of these methods of human brain analysis suffer from low throughput, which generates underpowered studies. Thus, the field is in need of an easy, inexpensive, and higher throughput method of analyzing synapse-level connectivity in the human brain.

Here, we demonstrate that neurons from small pieces of postmortem human brain tissue, which are more easily acquired from autopsy than whole brains, can be labeled and imaged at synapse-level resolution using the lipophilic dye DiI. DiI labeling is fast, inexpensive, and does not require special equipment yet generates high resolution three dimensional images of neuron morphology across a wide range of tissue ages and postmortem intervals. We demonstrate that DiI labeling is suitable for labeling most neuronal structures including axons, dendrites, spines, and presynaptic boutons. As proof of concept, we tested for age-dependent changes in hippocampal connectivity using 13 control brains across the lifespan. Interestingly, we find dendritic spine density and shape in hippocampal CA1 neurons is remarkably stable from infancy to old age. In contrast, DG mossy fiber presynaptic structure shows age-dependent structural plasticity and, to

our knowledge, this is the first analysis of DG mossy fiber synapses in human brain tissue. In summary, our newly proposed DiI-based labeling of postmortem human brain tissue should enable higher powered studies aimed at elucidating synapse-level structural changes underlying neuropsychiatric disorders.

2 | METHODS AND MATERIALS

2.1 | Tissue Preparation:

Human hippocampal tissue blocks were obtained through Utah's State Office of the Medical Examiner (OME). The brain tissue collection procedures are approved under an exemption (45CFR46.102(f)) from the Institutional Review Board (IRB) at the University of Utah. The age, sex, post-mortem interval (PMI), and manner of death for each case is summarized in Table 1. We used post-mortem hippocampus samples from 13 sudden death cases (10 males and 3 females). Based on toxicology reports, all the cases tested negative for acetone, isopropanol, methanol, cocaine, methamphetamine, morphine, and THC. Upon brain removal for autopsy at the OME, a 1.5 cm hippocampal block was immediately immersed in cold 4% (w/v) paraformaldehyde in 0.1 M Phosphate buffer (PB) (pH 7.4). After 1 hour of fixation, the hippocampal block was post-fixed in cold 4% paraformaldehyde plus 0.125% (v/v) glutaraldehyde in PB (pH 7.4) for 24 hours at 4°C. **Note:** this fixation time is optimized for 1.5 cm postmortem human tissue blocks. Tissue blocks with different sizes may require different fixation times. After post-fixation, 350 μm coronal sections were cut on a vibratome (Leica VT1200). Properly fixed brain slices may be stored in PB at 4°C for at least one month for DiI based labeling of dendritic spines and mossy fiber boutons.

2.2 | DiI-labeling:

Microscopic (particle size: ~10-20 μm) DiI crystals (Invitrogen, D282) were placed in the CA1 sub-region and supra-pyramidal blade of the DG for dendritic spine and mossy fiber bouton (MFB) analysis, respectively. A brain section was placed on a glass slide and the surface liquid was gently removed with a laboratory tissue. DiI crystals were manually placed using a pulled glass electrode (World Precision Instruments, 1B120F-4) under a dissecting microscope (5X). Slices were then placed in PB (pH 7.4) in a 12-well plate and incubated at 37°C. After 72 hours, sections were checked under a fluorescent microscope for sparse labeling of CA1 neurons and DG axons. Tissue sections with DiI labeling were coverslipped in PB and confocal imaging was performed within 48 hours.

2.3 | Confocal Imaging, Reconstruction, and Analysis:

Confocal imaging was performed on the CA1 and CA3 regions of the hippocampus for dendritic spines and MFBs, respectively (Figure 1). Images were acquired with a Zeiss LSM 710 confocal microscope using a 63X oil immersion objective (NA=1.4). We imaged basal and apical dendritic segments 70-100 μm from the soma. All images were obtained with a cubic voxel of 0.07 μm^3. Images of dendritic segments and MFBs were deconvolved using AutoQuant X3 (Bitplane, RRID: SCR_002465) using the following settings: total iterations: 10, save interval: 10, noise level: low, and noise value: 2. 3D spine and bouton modeling was performed using NeuroLucida 360 (MBF Bioscience). Dendritic segments were traced using Rayburst Crawl tracing method. Spines were classified into mushroom, stubby, thin and filopodia categories as described previously (Rodriguez, Ehlenberger, Dickstein, Hof, & Wearne, 2008).

2.5 | Statistics:

Statistical analyses were performed in Prism (GraphPad Software) and the SAS software package (www.sas.com). The coefficient of variation (CV) was used to characterize the variation of spine density among dendritic segments within a neuron. CV is the ratio of the standard deviation to the mean and shows the consistency of measurements in our experiments. To test age and PMI effects, mixed effect models were used to account for non-independence in the data introduced by the study of multiple neurons per case. For measures exhibiting significant age effects, inspection of the distribution of results prompted additional post hoc analyses to determine the specific effect of tissue from the youngest cases ($\leq$ 2 years) on the results. For these analyses, we removed these samples and re-ran the model, then also computed least squares means between the youngest case group and the rest of the sample to determine the magnitude of the difference, controlling for other predictors in the model (PMI effects and the presence of multiple neurons per case). Finally, significant age effects were also tested by introducing a non-linear age term to determine if a non-linear model more accurately explained the data. Two groups comparison between basal and apical spine parameters in adults were conducted through two-tailed unpaired t-test. Spine categories between basal and apical dendrites were compared through two-way ANOVA followed by Bonferroni's multiple comparison test.

3 | RESULTS

3.1 | DiI reliably labels dendritic spines in human tissue with long postmortem intervals

Dendritic spine analysis of human neurons is typically conducted on tissue that was fixed within a few hours of death (Benavides-Piccione et al., 2013; Merino-Serrais et al., 2013).

However, the requirement for extremely short postmortem intervals severely limits tissue collection and results in studies with low sample sizes. Therefore, we tested if spine densities of CA1 hippocampal neurons from tissues with a long postmortem interval are comparable to published spine densities from tissues with a very short postmortem interval. An overview of our DiI-labeled dendritic spine analysis in human post-mortem tissues is shown in Figure 1. Initially, we selected three cases (38, 57 and 68 years old) for which a 1.5 cm block of hippocampal tissue was immersion fixed 18 hours postmortem. We analyzed apical dendritic spines located 70-100 μm from the cell body from 3-5 neurons from each brain (Figure 2A-C). The mean apical spine density and spine head diameter ranged from 2.1 to 2.7 spines/μm and 0.38 to 0.39 μm, respectively, among these three cases (Figure 2D-E). These spine densities in neurons labeled from tissue fixed 18 hours postmortem is consistent with previously reported spine densities of human CA1 neurons in tissue fixed 1-3 hours postmortem (Merino-Serrais et al., 2013). This suggests that CA1 dendritic spine density is stable over much longer postmortem intervals than previously thought.

3.2 | The CA1 spine density variability among dendritic segments within a neuron is consistent across age

Next we sought to expand our data set and test if CA1 spine parameters vary with age and post-mortem intervals. We analyzed spine density and morphology from 11 cases with varying age from 5 months to 71 years old and postmortem intervals from 10 to 28 hours (Table 1). Because spine morphology and corresponding functional synapse properties vary between CA1 apical and basal dendrites in mice (Basu et al., 2017), we expanded our analyses to include CA1 apical and basal dendrites in humans. First, we investigated the reproducibility of DiI-based spine labeling by measuring the variability of spine density among dendritic segments within each neuron and

across ages. If membrane integrity and DiI diffusion is uniform in tissues irrespective of age and PMI, then we expect consistent variability of spine density in various dendritic segments across ages and PMI. We determined the variability of dendritic spine density among dendritic segments within each neuron using the coefficient of variation (CV). The mean % CV of spine density for basal dendritic segments varied from 10.06 % to 22.42 % across age (Figure 3A). The mean % CV of spine density for apical dendritic segments varied from 11.71 % to 23.81 % across age (Figure 3B). This data suggests that the tissue quality from a broad range of PMIs allows consistent dendritic spine analyses.

3.3 | CA1 dendritic spine parameters are stable in adults across a wide range of postmortem intervals

To test if CA1 spine density or morphology varies with age or postmortem interval time, we conducted a mixed model analysis of dendritic spine density, spine head diameter, and spine length with respect to age and postmortem interval (Figure 4 and Table 2). Our results indicate that postmortem interval does not have a significant effect on basal and apical spine density, spine head diameter, and spine length (Table 2). Given the wide age range of our cases we also conducted a linear regression analysis of dendritic spine parameters with respect to age. Here we found that age does not affect any parameter except apical spine density (Figure 4A, Table 2). Inspection of the distribution of apical spine density by age suggested substantial differences for cases $\leq$ 2 years old. A post-hoc analysis excluding cases < 2 years old indicates no significant effect of age on spine density demonstrating that the measurements from these youngest cases were responsible for the previous significant result. The least squares mean apical spine density for measurements from cases $\leq$ 2 years old was 3.23, significantly higher than the least squares mean of 2.21 found for the rest of the age distribution ($p<0.0001$). In summary, we find that CA1 apical spine density

is significantly greater in very young brains but that from age 23 to age 71 years old, both basal and apical CA1 spine density is stable.

It is known from rodent models that spine morphology and the synaptic strength of CA1 basal and apical dendrites is mediated through different molecular pathways (Basu et al., 2017; Brzdak et al., 2019). Thus, we tested if structural differences are present between CA1 apical and basal spines in human hippocampus. We pooled adult cases and compared apical and basal spine parameters. We find that apical spines have a significantly higher density and spine length but slightly smaller spine head diameter than basal spines (Figure 4A-F). Next, we classified spines into thin, stubby and mushroom categories. These well described spine morphology categories take into consideration spine length, head width, and neck width and are known to provide information about the maturity of the synapse. Mushroom spines, which have a high spine head width to neck ratio, are considered the most mature or recently potentiated synapses (Hering & Sheng, 2001). We found that apical dendrites had more thin spines and less stubby spines compared to the basal dendrites (Figure 4G) but, that apical and basal dendrites have about the same density of mushroom spines (Figure 4G). This suggests CA1 apical and basal dendrites have similar density of mature synapses in adult humans.

3.4 | Mossy fiber synapse morphology depends on age but not PMI.

The unmyelinated axons of dentate granule cells, called mossy fibers, form unique, multi-structured synapses with CA3 pyramidal cells and nearby GABA neurons. Here, a large main bouton synapses onto multi-headed spines of CA3 neurons and finger-like projections, called filopodia, originate from the main bouton to form synapses with GABAergic interneurons. While the main synapse provides strong mono-synaptic excitation to CA3 neurons, the filopodia synapses excite GABA neurons that, in turn, inhibit CA3 neurons (Scharfman, 2016). Mossy fiber filopodia-

mediated feed-forward inhibition has been shown to be important for learning and memory in mice (Guo et al., 2018; Ruediger et al., 2011) but mossy fiber synapses have never been examined in humans.

Here, we tested if presynaptic mossy fiber structures can be labelled with DiI in human post-mortem tissues. 3D reconstructed and neurolucida-modeled images of mossy fibers are shown in Figure 5A-C. We imaged and analyzed the number of filopodia, filopodia length and volume of the main bouton for 112 mossy fiber synapses from 10 cases (Table-1). Our results indicate that many morphological similarities exist between rodent and human mossy fiber synapses. Notably, similar to rodents, the mean number of filopodia per synapse is variable but consistently declines from neonates to adults. Interestingly, we noticed a clear trend for mossy fiber filopodia density to start out high in young children, decline to adulthood, and then start to increase again at age 70. Therefore, we tested if age and PMI had statistically significant impact on mossy fiber synapse structure. Mixed model results, adjusting for measurements from multiple neurons per case, are shown in Table 3. As with spine parameters, we found no significant effect of PMI on any parameter. However, age has significant effect on filopodia number ($p=0.0015$), filopodia length ($p=0.0006$) and bouton volume ($p=0.0031$). Inspection of the distributions by age suggested the effects of age may be non-linear. Additional analyses including a nonlinear age*age effect showed significance for filopodia number and bouton volume (Table 3). These results account for the increase in both of these parameters in measurements from both the oldest and youngest cases.

4 | DISCUSSION

4.1 | A DiI-based method for analyzing neuron structure in human post-mortem tissues

Pre- and post-synaptic structures are the physical traces of synapses and provide clues to synaptic strength yet analysis of micro-scale connectivity in human brain tissue is limited due to cumbersome methodology required. We describe DiI-based labeling of dendritic spines and axon boutons in human post-mortem tissue samples that has several advantages over existing methods. First, it is highly accurate yet faster, easier, more reliable, and less expensive than common methods. Second, it can be done in post-mortem human tissue samples within a broad range of post-mortem intervals (up to 28 hours), enabling larger sample sizes and higher-powered studies. Third, post-fixed tissues slices can be stored in PB up to a month providing a convenient time window for labeling. Fourth, although we only analyzed pre- and post-synaptic structures in the hippocampus, this method should be easily adapted to any other brain region. Overall, our proposed DiI-labelling should benefit researchers for the fast and accurate study of neuronal connectivity in healthy and disease conditions using human post-mortem tissues.

4.2 | Human CA1 spine parameters are stable throughout adulthood.

We 3D reconstructed and modeled 6196 basal and 6175 apical spines (total: 12371 spines) along the 5.284 mm of dendritic length (basal dendritic segments:109, apical dendritic segments:107) of human CA1 pyramidal neurons. One factor we assessed is spine density variability as measured by the co-efficient of variation (% CV) among dendritic segments within a neuron. We did this analysis to test if our labeling method produces consistent results for each case and across cases with different PMIs. We found that % CV is fairly consistent in our data sets, ranging from 10-20%. Some variance is naturally expected due to biology and some will be

introduced by methodology. We could not identify a similar technical analysis in the literature on data from rodent or human spine studies for comparison, but judging from reports where individual data points and standard deviation are reported, we estimate that our variance is similar to rodent studies conducted on optimally prepared tissue.

It is established that spine number and morphology provide a proxy for synapse density and strength. Previous studies in rodents, primates and human found that cortical dendritic spines are vulnerable to normal aging (Benavides-Piccione et al., 2013; Duan et al., 2003; Jacobs, Driscoll, & Schall, 1997; Wallace, Frankfurt, Arellanos, Inagaki, & Luine, 2007; Young, Ohm, Dumitriu, Rapp, & Morrison, 2014). Thus, we tested if aging also affects spines in human CA1 region of the hippocampus. Surprisingly, we found that spine density and morphology are stable throughout adulthood and old age. This agrees with a rodent model where CA1 dendritic spine density were not affected by age and sex (Markham, McKian, Stroup, & Juraska, 2005) and suggests that normal aging affects brain regions differentially.

4.3 | The structure of human mossy fiber boutons changes with age

The DG mossy fiber synapse is a major contributor to the storage of spatial memory (Holahan, Rekart, Sandoval, & Routtenberg, 2006; Ramirez-Amaya, Balderas, Sandoval, Escobar, & Bermudez-Rattoni, 2001). Thus, structural elucidation of mossy fiber boutons provides insights into spatial memory alteration. Here, we quantified the structure of mossy fiber synapses across ages and PMIs. As for CA1 spines, PMI has no effect on mossy fiber synapse structure, validating the methodology of including more cases in our study. In contrast and unlike CA1 spines, we find that age does significantly affect mossy fiber synapse structure (Table 3). The finding of increased filopodia density in our youngest cases is consistent with animal research (Wilke et al., 2013) and likely a developmental phenomenon with more motile filopodia still undergoing synapse

formation. Interestingly, we find that cases over age 70 also have an increase in mossy fiber filopodia density. Aging has been shown to impair spatial memory through increased excitability of CA3 neurons due to decreased GABAergic signaling or loss of GABAergic interneurons (Thome, Gray, Erickson, Lipa, & Barnes, 2016; Yassa et al., 2011). Because mossy fiber filopodia synapse with GABAergic interneurons, it is possible our finding reflects the attempt of a normal healthy brain to increase inhibitory drive to CA3 neurons via structural rearrangements of mossy fiber synapses. It will be interesting to follow up this study with increased sample sizes and analyses of mossy fiber structures in aged brain tissue of cases with known dementia or Alzheimer's disease to test if the diseased brain is unable to undergo this plasticity. Nonetheless, our study presents the first structural analysis of mossy fiber synapses in the human brain and suggests that mossy fiber synapses, in contrast to CA1 synapses, are particularly amenable to plasticity during aging.

4.5 | Summary:

In conclusion, our proposed DiI-labeling is applicable for accurate and higher throughput analysis of dendritic spines and mossy fiber synapses in human post-mortem tissue samples with broad post-mortem intervals (PMI). Using this method, it will be possible to study the alterations in pre- and post-synaptic structures throughout the brain in disease-specific human post-mortem tissue samples.

Conflict of Interest:

Authors declare no competing financial conflict of interests.

References:

Arellano, J. I., Espinosa, A., Fairen, A., Yuste, R., & DeFelipe, J. (2007). Non-synaptic dendritic spines in neocortex. *Neuroscience, 145*(2), 464-469. doi:10.1016/j.neuroscience.2006.12.015

Basu, R., Duan, X., Taylor, M. R., Martin, E. A., Muralidhar, S., Wang, Y., . . . Williams, M. E. (2017). Heterophilic Type II Cadherins Are Required for High-Magnitude Synaptic Potentiation in the Hippocampus. *Neuron, 96*(1), 160-176 e168. doi:10.1016/j.neuron.2017.09.009

Benavides-Piccione, R., Fernaud-Espinosa, I., Robles, V., Yuste, R., & DeFelipe, J. (2013). Age-based comparison of human dendritic spine structure using complete three-dimensional reconstructions. *Cereb Cortex, 23*(8), 1798-1810. doi:10.1093/cercor/bhs154

Berry, K. P., & Nedivi, E. (2017). Spine Dynamics: Are They All the Same? *Neuron, 96*(1), 43-55. doi:10.1016/j.neuron.2017.08.008

Brzdak, P., Wojcicka, O., Zareba-Koziol, M., Minge, D., Henneberger, C., Wlodarczyk, J., . . . Wojtowicz, T. (2019). Synaptic Potentiation at Basal and Apical Dendrites of Hippocampal Pyramidal Neurons Involves Activation of a Distinct Set of Extracellular and Intracellular Molecular Cues. *Cereb Cortex, 29*(1), 283-304. doi:10.1093/cercor/bhx324

Duan, H., Wearne, S. L., Rocher, A. B., Macedo, A., Morrison, J. H., & Hof, P. R. (2003). Age-related dendritic and spine changes in corticocortically projecting neurons in macaque monkeys. *Cereb Cortex, 13*(9), 950-961.

Forrest, M. P., Parnell, E., & Penzes, P. (2018). Dendritic structural plasticity and neuropsychiatric disease. *Nat Rev Neurosci, 19*(4), 215-234. doi:10.1038/nrn.2018.16

Guo, N., Soden, M. E., Herber, C., Kim, M. T., Besnard, A., Lin, P., . . . Sahay, A. (2018). Dentate granule cell recruitment of feedforward inhibition governs engram maintenance and remote memory generalization. *Nat Med, 24*(4), 438-449. doi:10.1038/nm.4491

Harris, K. M., Fiala, J. C., & Ostroff, L. (2003). Structural changes at dendritic spine synapses during long-term potentiation. *Philos Trans R Soc Lond B Biol Sci, 358*(1432), 745-748. doi:10.1098/rstb.2002.1254

Harris, K. M., Jensen, F. E., & Tsao, B. (1992). Three-dimensional structure of dendritic spines and synapses in rat hippocampus (CA1) at postnatal day 15 and adult ages: implications for the maturation of synaptic physiology and long-term potentiation. *J Neurosci, 12*(7), 2685-2705.

Hering, H., & Sheng, M. (2001). Dendritic spines: structure, dynamics and regulation. *Nat Rev Neurosci, 2*(12), 880-888. doi:10.1038/35104061

Holahan, M. R., Rekart, J. L., Sandoval, J., & Routtenberg, A. (2006). Spatial learning induces presynaptic structural remodeling in the hippocampal mossy fiber system of two rat strains. *Hippocampus, 16*(6), 560-570. doi:10.1002/hipo.20185

Jacobs, B., Driscoll, L., & Schall, M. (1997). Life-span dendritic and spine changes in areas 10 and 18 of human cortex: a quantitative Golgi study. *J Comp Neurol, 386*(4), 661-680.

Markham, J. A., McKian, K. P., Stroup, T. S., & Juraska, J. M. (2005). Sexually dimorphic aging of dendritic morphology in CA1 of hippocampus. *Hippocampus, 15*(1), 97-103. doi:10.1002/hipo.20034

Merino-Serrais, P., Benavides-Piccione, R., Blazquez-Llorca, L., Kastanauskaite, A., Rabano, A., Avila, J., & DeFelipe, J. (2013). The influence of phospho-tau on dendritic spines of cortical pyramidal neurons in patients with Alzheimer's disease. *Brain, 136*(Pt 6), 1913-1928. doi:10.1093/brain/awt088

Penzes, P., Cahill, M. E., Jones, K. A., VanLeeuwen, J. E., & Woolfrey, K. M. (2011). Dendritic spine pathology in neuropsychiatric disorders. *Nat Neurosci, 14*(3), 285-293. doi:10.1038/nn.2741

Radley, J. J., Rocher, A. B., Rodriguez, A., Ehlenberger, D. B., Dammann, M., McEwen, B. S., . . . Hof, P. R. (2008). Repeated stress alters dendritic spine morphology in the rat medial prefrontal cortex. *J Comp Neurol, 507*(1), 1141-1150. doi:10.1002/cne.21588

Ramirez-Amaya, V., Balderas, I., Sandoval, J., Escobar, M. L., & Bermudez-Rattoni, F. (2001). Spatial long-term memory is related to mossy fiber synaptogenesis. *J Neurosci, 21*(18), 7340-7348.

Rodriguez, A., Ehlenberger, D. B., Dickstein, D. L., Hof, P. R., & Wearne, S. L. (2008). Automated three-dimensional detection and shape classification of dendritic spines from fluorescence microscopy images. *PLoS One, 3*(4), e1997. doi:10.1371/journal.pone.0001997

Ruediger, S., Vittori, C., Bednarek, E., Genoud, C., Strata, P., Sacchetti, B., & Caroni, P. (2011). Learning-related feedforward inhibitory connectivity growth required for memory precision. *Nature, 473*(7348), 514-518. doi:10.1038/nature09946

Scharfman, H. E. (2016). The enigmatic mossy cell of the dentate gyrus. *Nat Rev Neurosci, 17*(9), 562-575. doi:10.1038/nrn.2016.87

Shen, H., Sesack, S. R., Toda, S., & Kalivas, P. W. (2008). Automated quantification of dendritic spine density and spine head diameter in medium spiny neurons of the nucleus accumbens. *Brain Struct Funct, 213*(1-2), 149-157. doi:10.1007/s00429-008-0184-2

Thome, A., Gray, D. T., Erickson, C. A., Lipa, P., & Barnes, C. A. (2016). Memory impairment in aged primates is associated with region-specific network dysfunction. *Mol Psychiatry, 21*(9), 1257-1262. doi:10.1038/mp.2015.160

Wallace, M., Frankfurt, M., Arellanos, A., Inagaki, T., & Luine, V. (2007). Impaired recognition memory and decreased prefrontal cortex spine density in aged female rats. *Ann N Y Acad Sci, 1097*, 54-57. doi:10.1196/annals.1379.026

Wilke, S. A., Antonios, J. K., Bushong, E. A., Badkoobehi, A., Malek, E., Hwang, M., . . . Ghosh, A. (2013). Deconstructing complexity: serial block-face electron microscopic analysis of the hippocampal mossy fiber synapse. *J Neurosci, 33*(2), 507-522. doi:10.1523/JNEUROSCI.1600-12.2013

Yassa, M. A., Lacy, J. W., Stark, S. M., Albert, M. S., Gallagher, M., & Stark, C. E. (2011). Pattern separation deficits associated with increased hippocampal CA3 and dentate gyrus activity in nondemented older adults. *Hippocampus, 21*(9), 968-979. doi:10.1002/hipo.20808

Young, M. E., Ohm, D. T., Dumitriu, D., Rapp, P. R., & Morrison, J. H. (2014). Differential effects of aging on dendritic spines in visual cortex and prefrontal cortex of the rhesus monkey. *Neuroscience, 274*, 33-43. doi:10.1016/j.neuroscience.2014.05.008

Tables

Table 1. Demographics of the cases.				
Sample ID	Age	Sex	PMI(Hours)	Manner of Death
U76*	4 Months	Male	25.5	Accident
U66	5 Months	Female	15	Accident
U51	2 Years	Female	18	Homicide
U78	23 Years	Male	12	Accident
U82	27 Years	Female	10	Accident
U71	38 Years	Male	18	Accident
U56	45 Years	Male	11	Natural
U58*	57 Years	Male	18	Natural
U63	57 Years	Male	18	Natural
U41	58 Years	Male	13	Natural
U61	68 Years	Male	18	Accident
U74	70 Years	Male	15.5	Accident
U67	71 Years	Male	28	Natural
*cases used for MFB analysis only.				

Table 2. Mixed model analyses to determine effects of age and PMI on spine characteristics, adjusting for multiple neurons measured on each case.				
Spine Density				
	Basal		Apical	
Variable	Estimate	p-value	Estimate	p-value
Age	-0.0024	0.65	-0.013	0.05
PMI	0.0021	0.94	0.034	0.28
Spine Head Diameter				
Variable	Basal		Apical	
	Estimate	p-value	Estimate	p-value
Age	0.00014	0.77	-5.79E-6	0.99
PMI	-0.00063	0.81	0.0018	0.27
Spine Length				
Variable	Basal		Apical	
	Estimate	p-value	Estimate	p-value
Age	-0.00086	0.65	-0.0017	0.17
PMI	0.0027	0.78	-0.0049	0.44

Table 3. Mixed model analyses of age and PMI effects on MFB parameters.		
Filopodia Number		
Variable	Estimate	p-value
Age	-0.066	0.0015
PMI	0.015	0.80
Filopodia Length		
Variable	Estimate	p-value
Age	-0.088	0.0006
PMI	-0.086	0.25
Mossy Fiber Bouton Volume		
Variable	Estimate	p-value
Age	-0.94	0.0031
PMI	0.62	0.54
Additional models allowing for non-linear effects of age.		
Filopodia Number		
Variable	Estimate	p-value
Age	-0.17	0.0050
Age*Age	0.0016	0.033
PMI	-0.081	0.19
Mossy Fiber Bouton Volume		
Variable	Estimate	p-value
Age	-2.48	0.0096
Age*Age	0.023	0.051
PMI	-0.72	0.46

Figure Legends:

Figure 1: Overview of DiI-labeling of Dendritic Spines in Human Fixed Tissue. **A.** Human hippocampal block (~1.5 cm) **B.** 350µm coronal slices of human hippocampus **C.** Nissl-stained slice of human hippocampus with its various sub-regions. Arrows: DiI microcrystal placement site. **D.** Confocal image of human CA1 pyramidal neurons labeled with DiI. **E.** A representative DiI-labeled basal dendritic segment **F.** A representative DiI-labeled apical dendritic segment. CA, Cornu Ammonis; DG, Dentate Gyrus.

Figure 2: 3D reconstruction and modeling of dendritic segments through Neurolucida 360 **A.** Apical dendritic segment with their representative model from 38-year-old case **B.** Apical dendritic segment with their representative model from 57-year-old case **C.** Apical dendritic segment with their representative model from 68-year-old case **D.** Distribution of apical spine density in various dendritic segments, red bar = mean **E.** Distribution of apical spine head diameter in various dendritic segments, red bar = mean.

Figure 3: Quantification of variance in basal and apical spine density within individual neuron across age. **A.** Age-wise distribution of co-efficient of variation (percentage) among various basal dendritic segments within each neuron. **B.** Age-wise distribution of co-efficient of variation (percentage) among various apical dendritic segments within each neuron.

Figure 4: Quantification of dendritic spine parameters across age **A.** The distribution of basal and apical spine density within each neuron across various age. **B.** Comparison of basal and apical spine density in adults, n= 30 neurons, two-tailed unpaired t-test. **C.** Spine head diameters of basal and apical spines within each neuron across various ages. **D.** Comparison of basal and apical spine head diameter in adults, n= 29-30 neurons, two-tailed unpaired t-test. **E.** Basal and apical spine

length within each neuron across various age. **F.** Comparison of basal and apical spine length in adults, n= 30 neurons, two-tailed unpaired t-test. **G.** Comparison of spine categories (%) between basal and apical dendritic segments, two-way ANOVA followed by Bonferroni's multiple comparison test, n= 31. All data represented as mean ± SEM. *, $p<0.05$; **, $p<0.01$; ***, $p<0.001$.

Figure 5: DiI-labeling, 3D reconstruction and quantification of mossy fiber bouton parameters in human post-mortem tissue. **A.** 3D-reconstructed mossy fiber boutons and their respective models through Neurolucida 360 in ≤2 Yrs, 20-40 Yrs and >40 Yrs age groups, respectively. **E**. Distribution of filopodia numbers across various age. **B.** Filopodia lengths across various age. **C**. Enclosed volume of MFB across various age. Each point represents the mean value per slice.

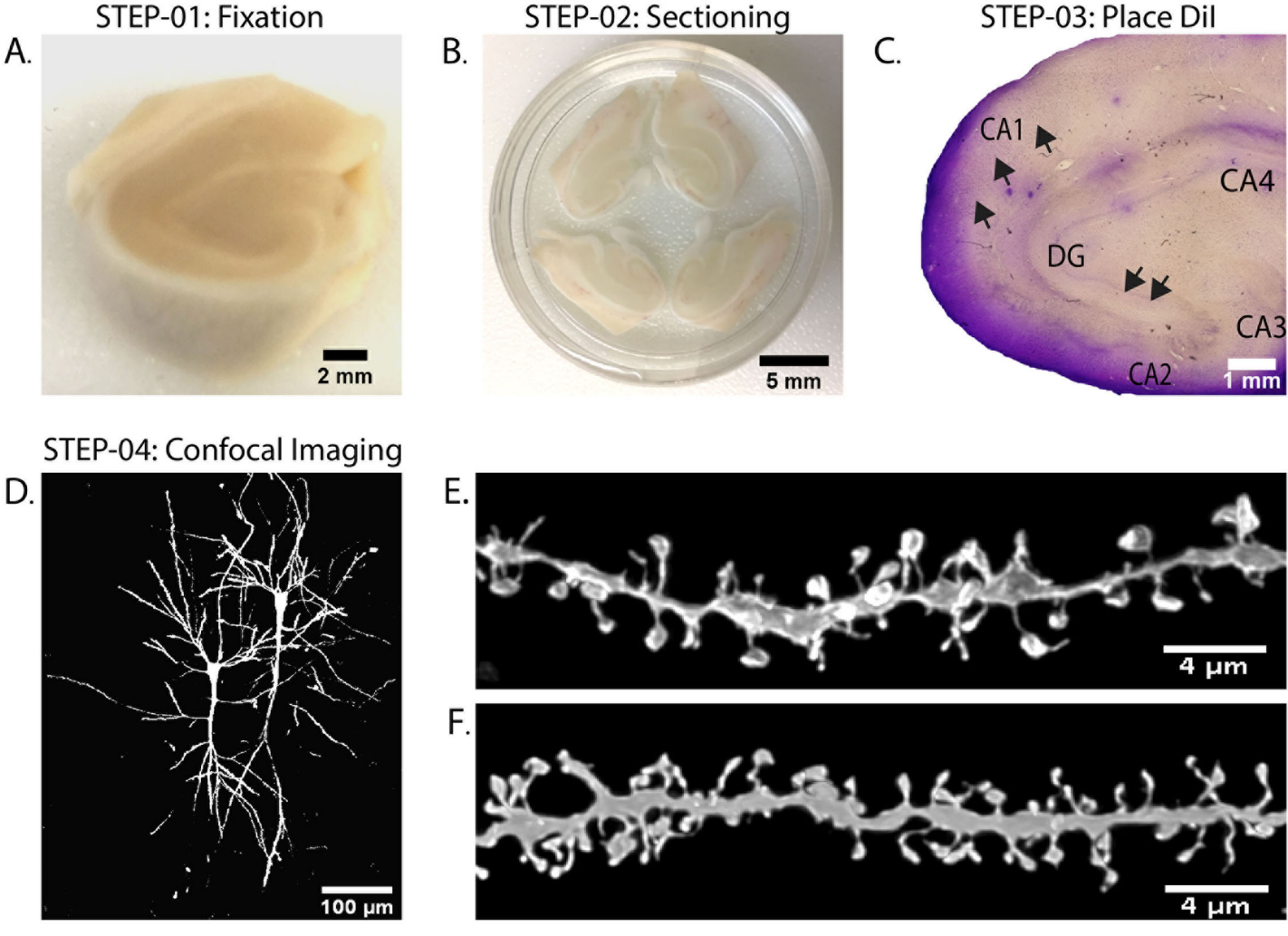
STEP-01: Fixation
A.
2 mm
STEP-02: Sectioning
B.
5 mm
STEP-03: Place DiI
C.
CA1
CA4
DG
CA3
CA2
1 mm
STEP-04: Confocal Imaging
D.
100 µm
E.
4 µm
F.
4 µm

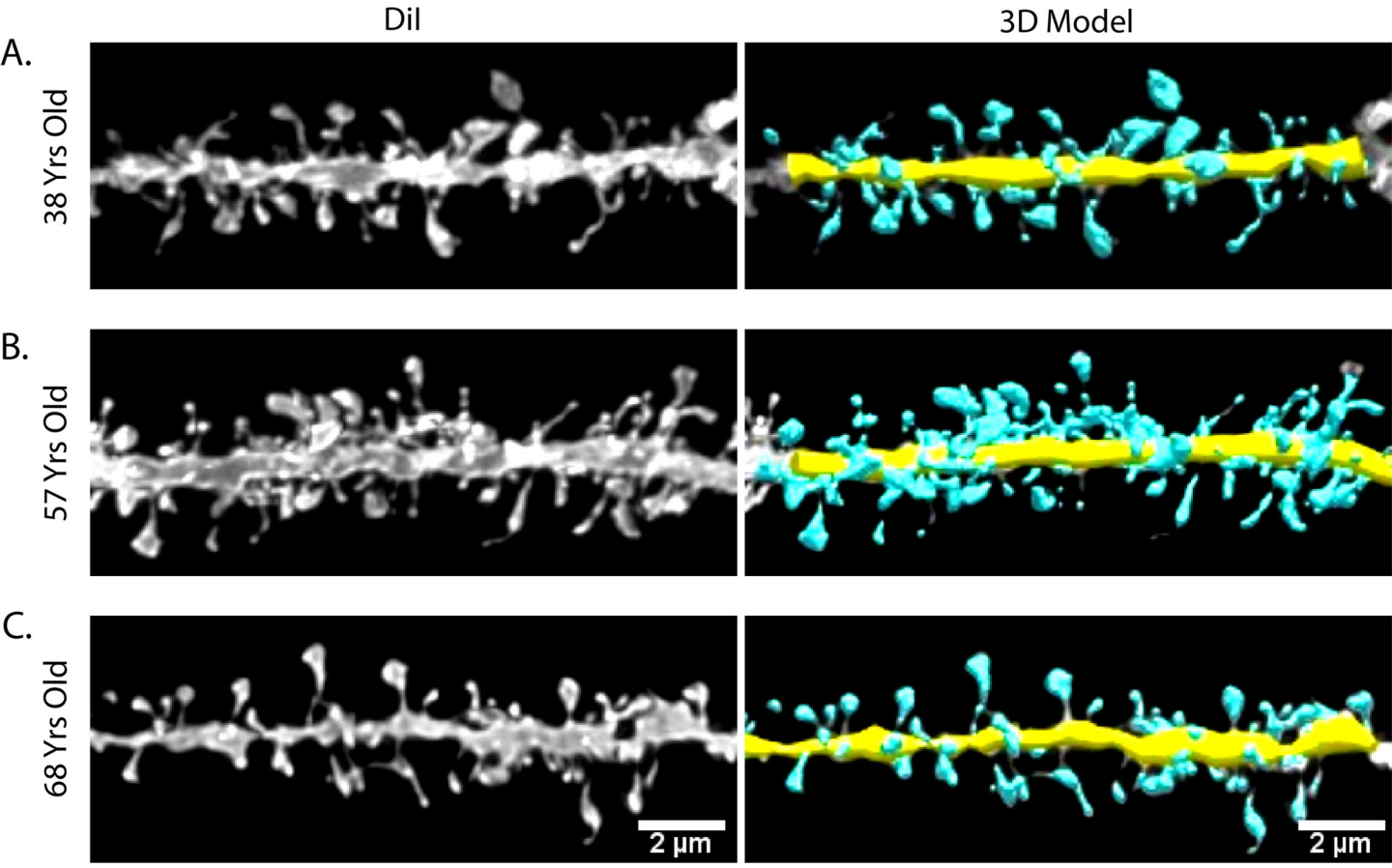
Dil
3D Model
A.
38 Yrs Old
B.
57 Yrs Old
C.
68 Yrs Old
2 µm
2 µm

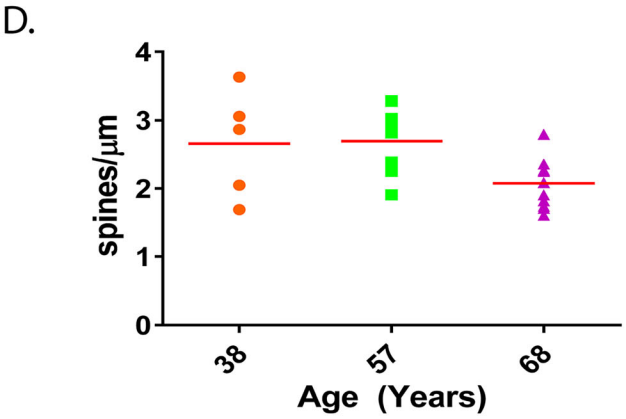
D.
spines/µm
0
1
2
3
4
38
57
68
Age (Years)

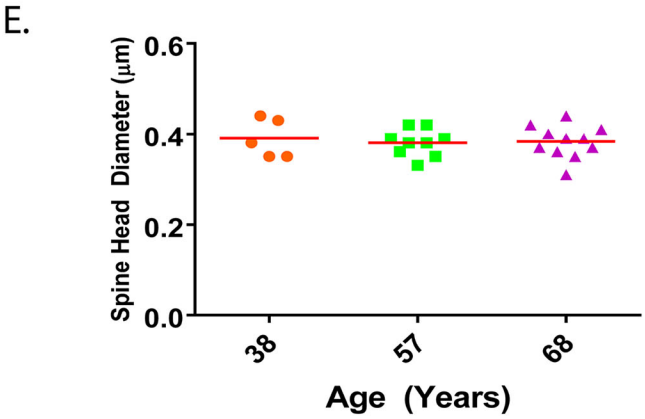
E.
Spine Head Diameter (µm)
0.0
0.2
0.4
0.6
38
57
68
Age (Years)

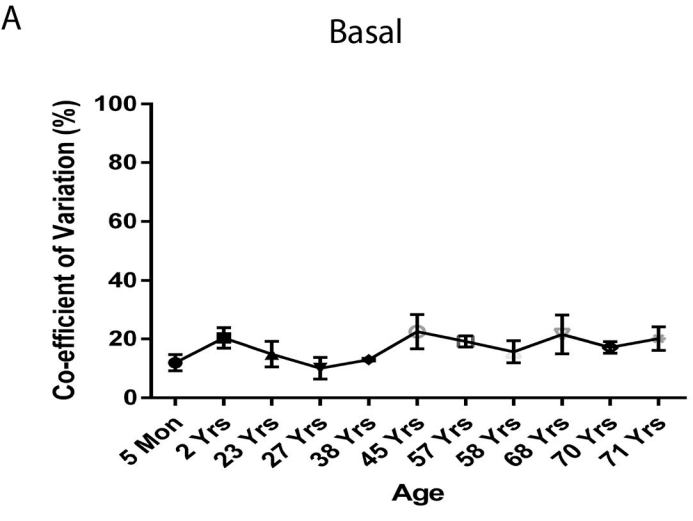
A
Basal
Co-efficient of Variation (%)
100
80
60
40
20
0
5 Mon
2 Yrs
23 Yrs
27 Yrs
38 Yrs
45 Yrs
57 Yrs
58 Yrs
68 Yrs
70 Yrs
71 Yrs
Age

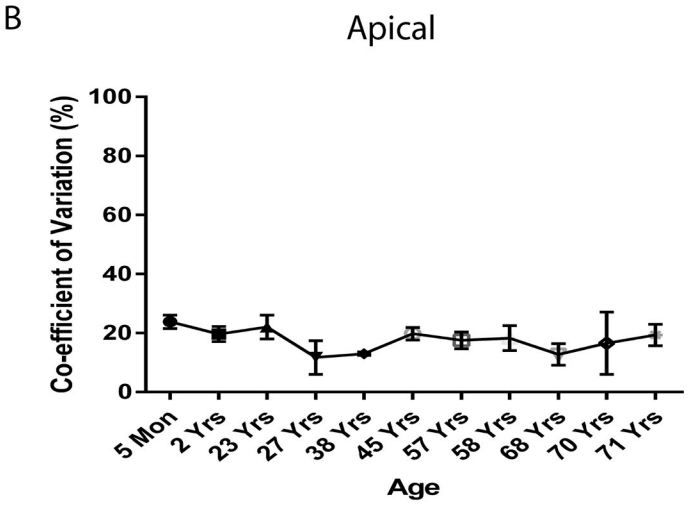
B
Apical
Co-efficient of Variation (%)
100
80
60
40
20
0
5 Mon
2 Yrs
23 Yrs
27 Yrs
38 Yrs
45 Yrs
57 Yrs
58 Yrs
68 Yrs
70 Yrs
71 Yrs
Age

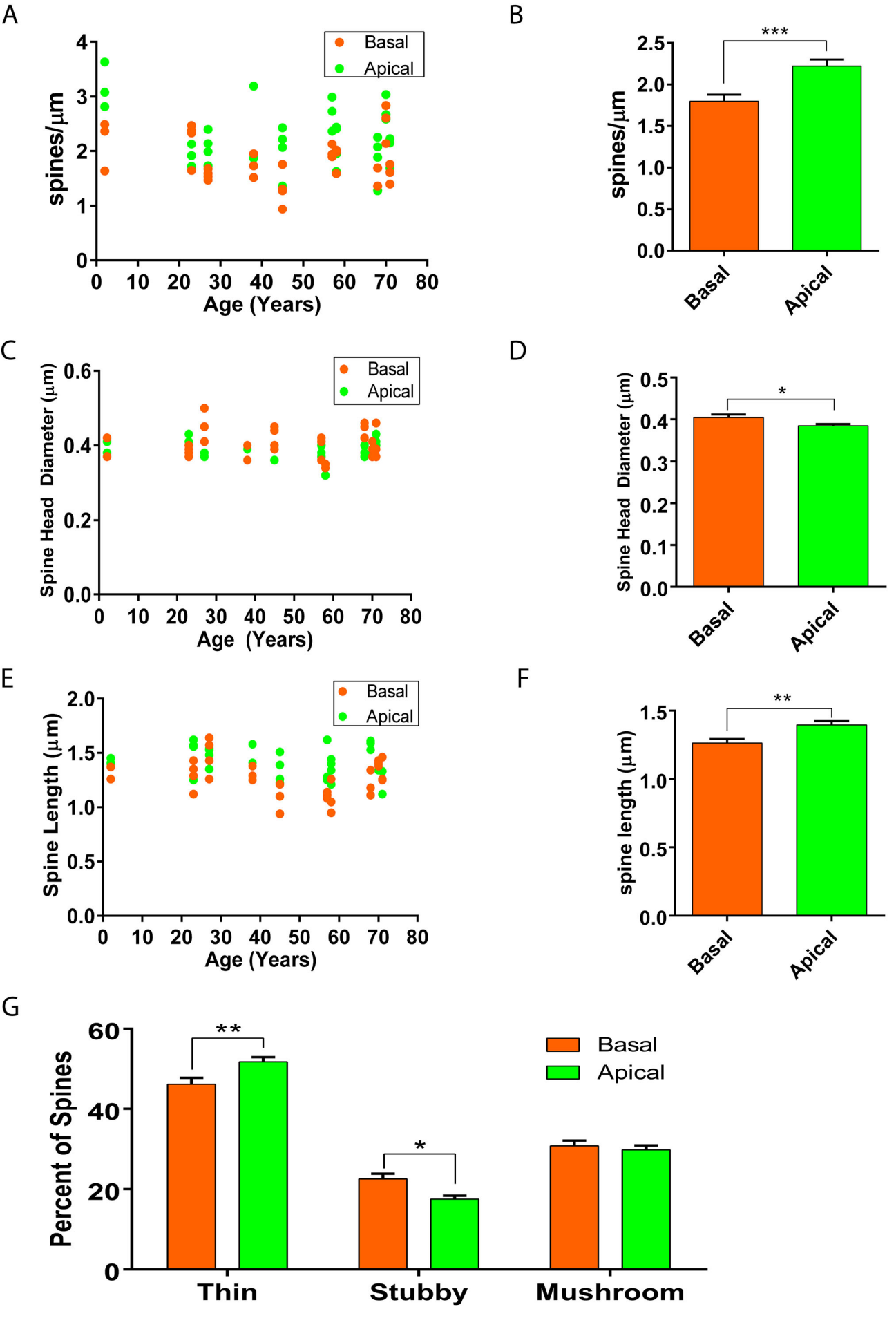
A
Basal
Apical
spines/µm
Age (Years)
B
***
spines/µm
Basal
Apical
C
Basal
Apical
Spine Head Diameter (µm)
Age (Years)
D
*
Spine Head Diameter (µm)
Basal
Apical
E
Basal
Apical
Spine Length (µm)
Age (Years)
F
**
spine length (µm)
Basal
Apical
G
**
*
Percent of Spines
Basal
Apical
Thin
Stubby
Mushroom

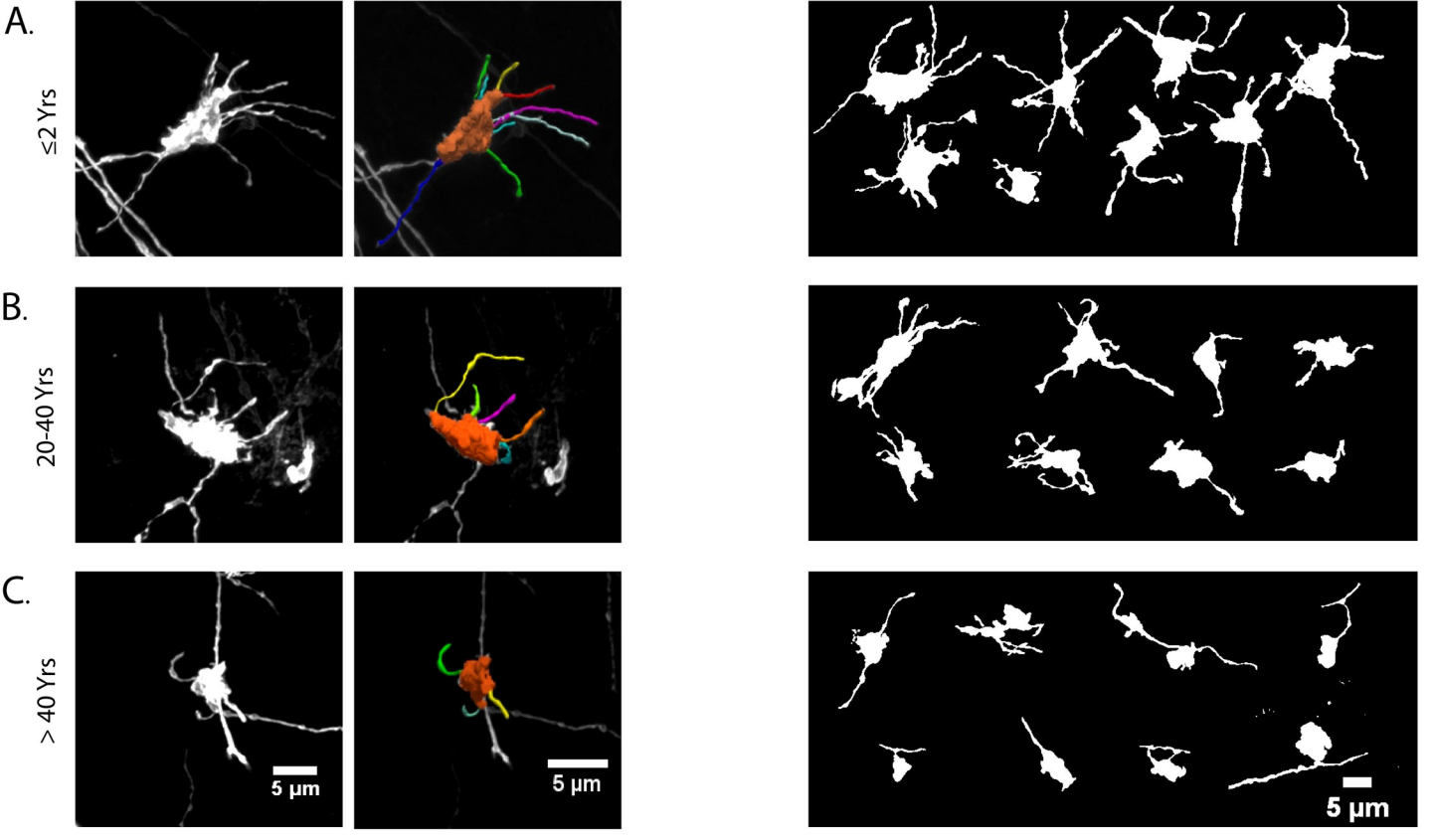
A.
≤2 Yrs
B.
20-40 Yrs
C.
> 40 Yrs
5 µm
5 µm
5 µm

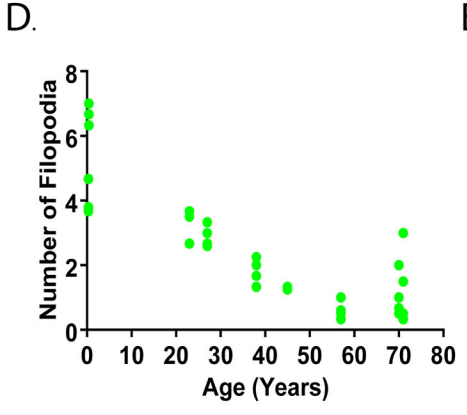
D.
Number of Filopodia
0
2
4
6
8
0 10 20 30 40 50 60 70 80
Age (Years)

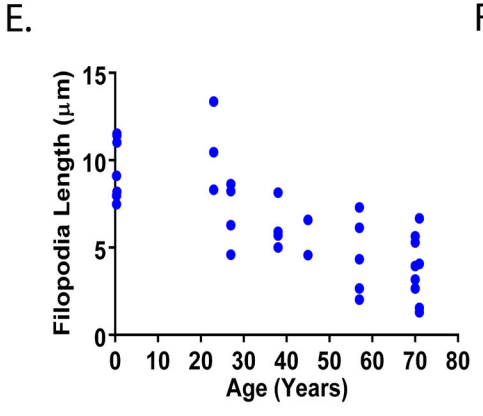
E.
Filopodia Length (µm)
0
5
10
15
0 10 20 30 40 50 60 70 80
Age (Years)

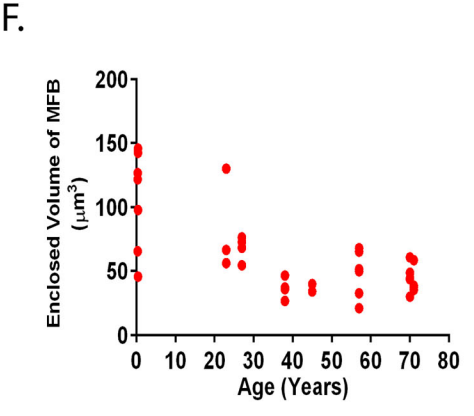
F.
Enclosed Volume of MFB
(µm³)
0
50
100
150
200
0 10 20 30 40 50 60 70 80
Age (Years)